

CORRELATION OF RUPTURE LIFE, CREEP RATE, AND MICROSTRUCTURE

FOR TYPE 304 STAINLESS STEEL*

R. W. Swindeman
Oak Ridge National Laboratory
Oak Ridge, Tennessee 37830

and

J. Moteff
University of Cincinnati
Cincinnati, Ohio 45221

ABSTRACT

The stress and temperature sensitivities of the rupture life (t_R) and secondary creep rate ($\dot{\epsilon}_s$) were examined in detail for a single heat of type 304 stainless steel (9T2796). Assuming that the rupture life (t_R) has a power law stress dependency, we observed relatively small differences in the stress exponent (n_R) over a broad range of stress and temperature. In contrast, large changes were observed for equivalent parameter (n_s) for secondary creep rate ($\dot{\epsilon}_s$). As a result of these differences, the Monkman-Grant correlation was sensitive to stress and temperature below 650°C. Metallurgical studies based on light and transmission electron microscopy suggested that the temperature and stress sensitivities of $\dot{\epsilon}_s$ at temperatures below 650°C were related to features of the substructure not present at higher temperature. Specifically, the presence of a fine dislocation network stabilized by precipitates altered the stress and temperature sensitivities relative to what might be expected from high-temperature studies.

INTRODUCTION

Structural components in high-temperature service usually experience variable loading conditions. Hence to assure that premature failure will not occur, the design analyst must use some parameter for summing damage. For nonreversing stresses time-under-stress,^{1,2} creep strain,³ and strain rate⁴ are sometimes used to sum damage; for fatigue loadings, cycles-to-failure related to stress,⁵ strain,⁶ and work energy⁷ are sometimes used; and for creep-fatigue two or more damage parameters are sometimes used.⁸

One of the difficulties in developing damage concepts for time-dependent failure is the need to verify that methods are valid for 10^9 s (3×10^5 h). Since fracture by creep or fatigue can be measured only once in a test, there is no direct way to measure damage without destroying the test specimen. Verification of a damage accumulation model therefore requires a large commitment of time and testing equipment. Crack growth rates can be measured under varying conditions, but the existence of cracks and the control of their growth in pressure boundary materials are not consistent with design to prevent crack initiation. In contrast, strain rate can be measured, does not require the preexistence of a crack, and on the basis of

*Work performed under DOE/RRT 189a OH048, *High-Temperature Structural Design Methods*.

the Monkman-Grant⁹ correlation between minimum creep rate and rupture life seems to be related to fracture. Consequently, several cumulative damage models as proposed by Majumdar,¹⁰ Ostergren,¹¹ and Manjoine⁴ use the strain-rate response to estimate damage and predict fracture.

To place confidence in predictions that are based on strain rate as a measure of damage, it is necessary to establish that the stress and temperature dependences of the secondary creep rate ($\dot{\epsilon}_s$) and the rupture life (t_R) are similar. Further, it should also be demonstrated that this similarity persists for conditions for which fracture data are meager.

This paper examines the stress and temperature dependences of $\dot{\epsilon}_s$ and t_R for a heat of type 304 stainless steel on which a very large data base exists. We also examine the validity of the Monkman-Grant correlation and show how stress and temperature influences this correlation. Finally, metallurgical factors that influence creep rate and rupture life are discussed.

DATA BASE AND ANALYSIS METHODS

The data base consisted of several hundred tensile and creep-rupture tests, which covered times in the range 1 to 1.4×10^8 s and temperatures from 427 to 871°C. Data included 25-mm plate and 16-mm bar of a reference heat of type 304 stainless steel (9T2796). Although not used directly in the correlations, data on 51-mm plate extending to 2.2×10^8 s were of considerable value in estimating the behavioral trends at long times.

Most of the data on which calculations were based have been published elsewhere.¹²⁻¹⁴ In some instances engineering stresses were reported, while in others true stresses were reported. Our tensile stress data represent the saturation flow stresses obtained from a fit of the Voce equation to the true stress vs true strain data.¹⁴ The "rupture life" in tensile tests represents the time between the ultimate strength and fracture.¹² The creep stress data represent true stresses obtained by multiplying engineering creep stress by the factor $1 + e_p$ where e_p is the inelastic strain about halfway through the test.¹² Below 650°C e_p was dominated by the plastic loading strain, and the stress changed by less than 10% during the creep test. Above 650°C e_p was dominated by the creep strain, which was in the 30-60% range.

The stress sensitivities of $\dot{\epsilon}_s$ and t_R were evaluated with the assumption that power relations existed between both $\dot{\epsilon}_s$ and σ/E and t_R and σ/E . Thus, for any isothermal pair of points at $(\sigma_1/E, \dot{\epsilon}_{s1})$ and $(\sigma_2/E, \dot{\epsilon}_{s2})$, the stress exponent for creep rate, n_s , was calculated:¹

$$n_s = \frac{\ln(\dot{\epsilon}_{s1}/\dot{\epsilon}_{s2})}{\ln(\sigma_2/\sigma_1)} \dots \dots \dots (1)$$

Similarly, the stress exponent for rupture, n_R , was calculated:

$$n_R = \left| \frac{\ln(t_{R2}/t_{R1})}{\ln(\sigma_2/\sigma_1)} \right| \dots \dots \dots (2)$$

Data pairs were read from visually smoothed curves through the experimental points. The two stresses, σ_1/E and σ_2/E , were generally spaced about 0.15 log cycles apart.

RESULTS

Contour Maps

Figure 1 shows a contour map of the variation in the stress exponent for rupture (n_R) with the modulus-compensated stress (σ/E) and the temperature (T). Over most of the range where data are available n_R falls between 6 and 8. A region also exists around 600°C for σ/E less than 10^{-3} where n_R appears to increase above 8. The stress exponent for creep rate, n_s , exhibits a more complicated pattern as σ/E and T are varied. This pattern is shown in Fig. 2. At temperatures above 600°C n_s usually falls in the range 6 to 8. Thus, n_s and n_R agree. Higher n_s values are observed for high σ/E , and this pattern is also consistent with the trend for n_R . Below 650°C the n_s values differ from the n_R values. For example, between 540 and 600°C the n_s values are in the range 8 to 10 compared to n_s values in the range 6 to 8. Below 540°C and at low stresses the n_s values seem to decrease, but no data exist for n_R ; hence, no comparison is possible.

Correlations Between Strain Rate and Rupture Life

Comparison of data in Figs. 1 and 2 leads us to conclude that the stress and temperature dependencies of \dot{e}_s and t_R are similar above 650°C, at least over the range where data are available. Thus, it should be possible to use \dot{e}_s as a parameter to sum damage for varying stresses. It is equally apparent that the stress and temperature dependencies of \dot{e}_s and t_R are dissimilar below 650°C. Even so, it might be possible to sum damage with \dot{e}_s if we can understand the functional relationship between \dot{e}_s and t_R . If we assume that both \dot{e}_s and $1/t_R$ can be represented by power law expressions, then we can eliminate stress and show that for isothermal conditions:

$$t_R \propto \dot{e}_s^{-m} \dots \dots \dots (3)$$

where m is the slope of the Monkman-Grant plot and is equal to the ratio n_R/n_s . In Fig. 3 we plot $\log t_R$ vs $\log \dot{e}_s$ for temperatures of 816, 760, 704, 649, 593, 538, and 482°C. Data at the two highest temperatures plot as a straight line with a slope close to -1.0 (Fig. 3, Curve A). This trend covers six decades of \dot{e}_s and t_R . Data for 704°C more-or-less follow a trend similar to data at higher temperatures (Fig. 3, Curve B).

Data for 649°C fall near Curve C in Fig. 3. Here the data at high \dot{e}_s follow the $m = 1.0$ trend, but for rates below $10^{-5}/s$ the slope decreases slightly and is closer to -0.97 . The data base at 593°C is very extensive and covers approximately ten decades of \dot{e}_s (Fig. 3, Curve D). The curve starts out with a slope near -1.0 then shifts to a slope of near -0.88 until \dot{e}_s is $10^{-8}/s$. Below this \dot{e}_s the slope decreases precipitously and around $10^{-10}/s$ the value of m is 0.5 or less. The large scatter in the data is attributable to grain size variations in the material. Finer grain sizes

(80 μm) lead to greater rupture lives than coarser grain sizes (180 μm). Relative to the high-temperature Monkman-Grant Curve A, Curve D at 593°C has shifted downward by a factor of two at high strain rates and considerable more at very low strain rates.

Data for 538°C are plotted in Fig. 3 and fall near Curve E. Here we see that $m = 1.0$ for high $\dot{\epsilon}_s$ and 0.83 for lower strain rates. If the trend continued the Monkman-Grant curve for 538°C would intersect the curve for 593°C at a strain rate around $10^{-10}/\text{s}$. No data are available to verify this. Difficulties occur in defining the $\dot{\epsilon}_s$ values at 482°C because the creep curves have tertiary creep character. Hence, the data plotted along Curve F in Fig. 3 for 482°C should be considered as tenuous. Over much of the data range m is near 0.75 at 482°C. Compared to the high-temperature Monkman-Grant Curve A, the curve at 482°C is displaced toward lower t_R by more than a decade at low strain rates.

In summary, at high strain rates (10^{-4} to $10^{-1}/\text{s}$) the $\log t_R$ vs $\log \dot{\epsilon}_s$ plots follow the $m = 1.0$ trend for all temperatures, but there is a small decrease in t_R with decreasing temperature for the same $\dot{\epsilon}_s$. Assuming that $n_R = n_s$ at high $\dot{\epsilon}_s$ values, it follows that the decrease in t_R is associated with a decrease in the post-uniform strain in the tensile tests with decreasing temperature. At intermediate strain rates (10^{-9} to $10^{-4}/\text{s}$) the $\log t_R$ vs $\log \dot{\epsilon}_s$ plots fan out, with m decreasing and t_R decreasing with decreasing temperature for the same $\dot{\epsilon}_s$. This implies that n_R is less than n_s , which is consistent with the contour maps shown in Figs. 1 and 2. Very low-strain-rate data at 593°C exhibit low n values, but we do not know whether the other curves bend over. This is important from an engineering viewpoint since most of the creep-rupture damage is accumulated at strain rates in the range 10^{-11} to $10^{-8}/\text{s}$, while most fatigue damage is accumulated at rates in the range 10^{-6} to $10^{-5}/\text{s}$. Thus, service conditions often enter into the region of poorly defined behavior.

An alternative approach to the use of strain rate as a parameter in damage accumulation is the linear strain parameter. This is defined as the product $\dot{\epsilon}_s t_R$ and is sometimes called the "plasticity resource."^{15,16} Whereas the Monkman-Grant approach attempts to "predict" rupture from the "known" strain rate, the linear strain parameter is not predictive since both the $\dot{\epsilon}_s$ and t_R must be known to evaluate the parameter. The parameter $\dot{\epsilon}_s t_R$ is highly sensitive to differences in the stress and temperature sensitivities of $\dot{\epsilon}_s$ and t_R . Assuming power law behavior:

$$\dot{\epsilon}_s t_R \propto (\sigma/E) n_s^{-n_R} \dots \dots \dots (4)$$

Hence, a plot of $\log \dot{\epsilon}_s t_R$ vs $\log \sigma/E$ will define a curve with a slope that reflects the difference $n_s - n_R$. Data are plotted in Fig. 4. Here we see that at high temperatures the isothermal data fall on horizontal lines. This implies that $n_s = n_R$. At lower temperatures data fall on lines that exhibit slopes between 1 and 2. At low stresses the data trend is not well defined, but there is some evidence at 593°C of a very steep slope. The linear strain parameter is highly variable with stress and temperature, and its "predictive" capabilities for very low stresses are questionable.

Metallurgical Features

The features of the metallurgical substructure (Figs. 5-8) are more-or-less consistent with the observed mechanical behavior. In the region of stress and temperature where $n_g = n_R$, subgrains form (Fig. 5) and precipitate when present consists of large and blocky particles. Matrix carbide particles exceed $0.1 \mu\text{m}$ (Fig. 6), and grain boundary carbide particles are $0.5 \mu\text{m}$ in size (Fig. 7). Failure is always intergranular and initiated at triple points and twin grain boundary intersections. At the lowest stresses we suspect that microvoid formation and coalescence are active, but we have not studied them quantitatively. Below 650°C the evolution of substructure is complex, and this complexity probably produces the variation of n_g with stress and temperature. At high stresses cells generally form and grain boundary carbides are often present. These carbide particles quickly grow to a size in the range 0.1 to $0.2 \mu\text{m}$. Matrix carbides may be absent or relatively fine ($<0.05 \mu\text{m}$). Failure is predominantly intergranular with wedge-type cracks nucleating at grain boundary triple points. When σ/E values fall below 0.001 no cells or subgrains form. Rather, the substructure consists of a fine network of dislocations perhaps stabilized by the fine distribution of carbide, as suggested by Hopkin and Taylor.¹⁷ The change in dislocation density appears to be about 50% higher than for comparable σ/E values at higher temperatures (Fig. 8). Large grain boundary carbide particles (0.1 to $0.4 \mu\text{m}$) are present, and failure is intergranular with wedge-type cracking. At stresses below the range where rupture data are available, the substructure consists of coarse dislocation networks decorated by a fine precipitate. This is essentially the same substructure that developed in simply aged material.¹⁸ Below 510°C matrix carbides are not observed to 36 Ms, and even grain boundaries are relatively free of precipitates. Again, failure is initiated by wedge cracks at grain boundaries, but often these cracks are blunted by additional plastic deformation in the final stages of creep rupture. Thus, the transgranular creep rupture described by Ashby and coworkers^{19,20} dominates.

Cracking patterns were studied in approximately 50 specimens. Data were obtained in several categories including crack density, ratio of the number of triple point cracks to total cracks, ratio of crack length to grain boundary length, and the orientation angle between the crack and the stress axis. Most of the data were obtained by Bhargava, who used procedures developed by Nahm, Michel, and Moteff.^{21,22}

No cracks were observed in specimens with less than 3% total strain, and when cracks were present both the crack density and the crack length increased with creep strain. The orientation angle between the cracks and the stress axis increased with decreasing strain rate and was usually in the range 50 to 80° . Grain boundary migration was sometimes observed above 593°C , while recrystallization was sometimes observed above 704°C . These observations are consistent with literature data.^{22,23}

DISCUSSION

The strong stress and temperature dependencies of $\log t_R$ vs $\log \dot{\epsilon}_g$ and $\log \dot{\epsilon}_g t_R$ vs $\log \sigma/E$ are not unique to heat 9T2796. Indeed, we have analyzed data on two other heats of type 304 stainless steel and find similar trends at 593 and 649°C . To some extent the rupture life is influenced by the pre-

precipitation of the $M_{23}C_6$ carbide, and this influence shows up as a slight cusp in the $\log t_R$ vs $\log \sigma$ curve.¹² However, the variations in the stress and temperature dependencies of t_R are not nearly as severe as the variations for $\dot{\epsilon}_s$. The reasons for high n_s values around 600°C are not altogether clear. One possibility is that the precipitation-stabilized dislocation network acts in much the same way as precipitation hardening. If so, we could speak of an internal stress, σ_i , which is relatively constant for a given temperature. Then $\dot{\epsilon}_s$ in terms of an effective stress is

$$\dot{\epsilon}_s = f\left\{T, [(\sigma - \sigma_i)/E]\right\} \dots \dots \dots (5)$$

where $[(\sigma - \sigma_i)/E]$ is the effective stress (Lagneborg,²⁴ Wilshire,²⁵ and Nix and coworkers²⁶). As the carbide particles grow in size and particle spacing increases, σ_i could change. If it does not, then when the applied stress is below σ_i , the secondary creep rate would be zero (if we ignore the contribution of grain boundary sliding, diffusional flow, and climb over the particles). Creep would then consist of only transient and tertiary components. However, at 649°C subgrains sometimes form and the matrix carbide particle size is large. Thus, diffusion and thermal recovery proceed rapidly, and the possibility of hardening as outlined above is questionable. Tanaka and Shinoda²⁷ link the creep strength at 650°C to the carbide particle size and spacing, which suggests that the carbide continues to influence σ_i . Our data on carbide particle sizes agree well with weak heats of 18-8 stainless steel studied by Tanaka and Shinoda²⁷ and Étienne, Dortland, and Zeedijk.²⁸ However, we emphasize that it is not the precipitate alone that produces the hardening. We say this because, as pointed out by Barnby²⁹ and Sikka et al.,¹⁸ the results from creep tests on aged materials that develop precipitates show either a loss or no change in creep strength relative to the nonaged condition. Thus, dynamic precipitation gives rise to the strengthening effect of σ_i . Precipitation kinetics with or without strain is qualitatively understood in type 304 stainless steel. We know, for example, that the matrix carbide develops more rapidly under monotonic and cyclic strains than under simple aging. We do not know whether the dislocation substructure produced by dynamic precipitation is different from the substructure developed by creep testing aged material. This would be of considerable interest.

An alternative explanation for high n_s values could be solid-solution strengthening, as proposed recently by Miller and Sherby.³⁰ Here the solid solution is produced by a Cottrell atmosphere drag force on dislocations. The magnitude of the effect is a function of a temperature-compensated strain rate $\dot{\epsilon}_s/\theta$, where θ is given by $\exp(-Q/RT)$ and Q is the activation energy associated with the species that produces the Cottrell atmosphere. Miller and Sherby³⁰ propose a "drag" rather than a "friction" strengthening effect. Hence, instead of Eq. (5) we have

$$\dot{\epsilon}_s = f\left\{T, \frac{\sigma}{\sigma_D(T, \dot{\epsilon}_s)}\right\} \dots \dots \dots (6)$$

where σ_D is the strengthening effect due to drag. This is a very powerful modification, since it is possible to let $\sigma_D(T, \dot{\epsilon}_s)$ reflect interstitial,

substitutional, and interaction solid-solution hardening effects. It is also possible to introduce a dependence of $\sigma_D(T, \dot{\epsilon}_s)$ on the total deformation as well. With this much flexibility the complex variation of n_s could be modeled to any degree of accuracy. If we restrict ourselves to only one solution strengthening mechanism, then by use of the treatment outlined by Miller and Sherby,³⁰ n_s should be a unique function of σ/E and not vary with temperature for constant σ/E . If we assume that more than one solution hardening mechanism is present and that Eq. (6) could be used to represent $\dot{\epsilon}_s$, then we would expect that the slope of $\log t_R$ vs $\dot{\epsilon}_s$ might return to -1 at sufficiently low stresses. Similarly, the linear creep component $\dot{\epsilon}_s t_R$ should always exhibit nonzero values and perhaps even increase at low stresses. Eventually, new deformation mechanisms and failure mechanisms may enter the picture, as suggested by Ashby and coworkers.^{19,20} However, it is beyond the scope of our experimental data to assess these new problems. Nevertheless, Morris and Harris³¹ recently suggest that a deformation "mechanism based on dislocation locking by solute atom complexes" occurs in type 316 stainless steel around 525°C. Hence, apparently more data are being obtained for this temperature range.

CONCLUSIONS

1. Above 650°C the stress and temperature dependences of the secondary creep rate ($\dot{\epsilon}_s$) and the rupture life (t_R) are similar. The product $\dot{\epsilon}_s t_R$ is relatively constant, and the exponent in the Monkman-Grant relation is close to 1.0. These observations apply to at least 4×10^6 s.

2. Below 650°C the stress and temperature dependences of $\dot{\epsilon}_s$ and t_R often differ. The product $\dot{\epsilon}_s t_R$ decreases stress and decreasing temperature. The exponent in the Monkman-Grant changes from 1.0 toward zero as temperature and $\dot{\epsilon}_s$ decrease. These observations apply in the range 10^4 to 10^8 s.

3. The fact that $\dot{\epsilon}_s$ - t_R correlations are stress and temperature sensitive below 650°C is due primarily to changes in the $\dot{\epsilon}_s$ behavior rather than in the rupture mechanism. Changes in the $\dot{\epsilon}_s$ behavior could be attributed to either a high internal stress, σ_i , produced by the development or precipitation-stabilization dislocation network or to a somewhat complex solute hardening mechanism.

4. Although grain boundary carbide particle sizes and crack densities change over our range of stress and temperature, there was no evidence to indicate that these features of microstructure greatly influence the stress and temperature dependence of the rupture life.

5. Above 650°C $\dot{\epsilon}_s$ can be a parameter for a damage accumulation model. Below 650°C $\dot{\epsilon}_s$ can be used to sum damage over the range of stress and times where the relation between $\dot{\epsilon}_s$ and t_R is known.

REFERENCES

1. E. L. Robinson, *Trans. ASME*, 1952, vol. 74, pp. 777-80.
2. S. Taira, *Creep in Structures*, pp. 96-124, Academic Press, New York, 1962.

3. D. A. Spera, Report No. NASA TN D-5489, NASA-Lewis Laboratories, Cleveland, Ohio, 1969.
4. M. J. Manjoine, *J. Eng. Mater. Technol.*, 1975, vol. 97, pp. 156-61.
5. M. A. Minor, *J. Appl. Mech.*, 1945, vol. 12, pp. 159-65.
6. L. F. Coffin, Jr., *Trans. ASME*, 1954, vol. 76, pp. 931-50.
7. J. D. Morrow, *Internal Friction, Damping, and Cyclic Plasticity STP 378*, pp. 45-87, American Society for Testing and Materials, Philadelphia, 1965.
8. R. D. Campbell, *Advances in Design for Elevated Temperature Environment*, pp. 45-56, American Society of Mechanical Engineer, New York, 1975.
9. F. C. Monkman and N. J. Grant, *Proc. Am. Soc. Test. Mater.*, 1956, vol. 56 pp. 593-605.
10. S. Majumdar and P. S. Maiya, *Symposium on Creep-Fatigue Interaction*, pp. 323-44, American Society of Mechanical Engineers, 1976.
11. W. J. Ostergren and E. Krempl, General Electric Company, Schenectady, and Rennslear Polytechnic Institute, Troy, paper 78-PVP-63, ASME/CSME Pressure Vessel and Piping Conference, Montreal, Canada, June 25-30, 1978.
12. R. W. Swindeman, *Structural Materials for Service at Elevated Temperatures in Nuclear Power Generation*, pp. 1-30, American Society of Mechanical Engineers, New York, 1975.
13. R. V. Bhargava, J. Moteff, and R. W. Swindeman, *Structural Materials for Service at Elevated Temperatures in Nuclear Power Generation*, pp. 31-54, American Society of Mechanical Engineers, New York, 1975.
14. R. W. Swindeman, *J. Eng. Mater. Technol.*, 1975, vol. 98, pp. 98-106.
15. V. S. Ivanova, *Zavod. Lab*, 1955, vol. 21, pp. 212-16.
16. M. K. Booker, C. R. Brinkman, and V. K. Sikka, *Structural Materials for Service at Elevated Temperatures in Nuclear Power Generation*, pp 108-45, American Society for Mechanical Engineers, New York, 1975.
17. L.M.T. Hopkin and L. H. Taylor, *J. Iron Steel Inst. London*, 1967, vol. 205 pp. 17-27.
18. V. K. Sikka, C. R. Brinkman, and H. E. McCoy, Jr., *Structural Materials for Service at Elevated Temperatures in Nuclear Power Generation*, pp. 316-50, American Society of Mechanical Engineers, New York, 1975.
19. M. F. Ashby, Report No. CUED/C/MATA/TR.34, Cambridge University, Cambridge, England (undated).
20. M. F. Ashby, R. J. Fields, and T. Weerasooyia, Report No. CUED/C/MATS/TR.47, Cambridge University, Cambridge, England (undated).

21. D. J. Michel, H. Nahm, and J. Moteff, *Mater. Sci.*, 1973, vol. 11, pp. 97–102.
22. H. Nahm, D. J. Michel, and J. Moteff, *J. Mater. Sci.*, 1968, vol. 3, pp. 596–602.
23. F. Garofalo, *Fundamentals of Creep and Creep-Rupture in Metals*, pp. 221–26, MacMillan Company, New York, 1968.
24. R. Lagneborg, *J. Mater. Sci.*, 1968, vol. 3, pp. 596–602.
25. J. D. Parker and B. Wilshire, *Met. Sci.*, 1975, vol. 9, pp. 249–52.
26. R. W. Lund and W. D. Nix, *Acta Metall.*, 1976, vol. 24, pp. 469–81.
27. T. Shinoda and R. Tanaka, *Nippon Kinzoku Gakkai Kaiho*, 1962, vol. 11, pp. 180–91.
28. C. F. Etienne, W. Dortland, and H. B. Zeedijk, *Creep and Fatigue in Elevated Temperature Applications*, pp. 225.1–225.9, The Institute of Mechanical Engineers, London, England, 1975.
29. J. T. Barnby, *J. Iron and Steel Inst. London*, 1966, vol. 204, pp. 23–27.
30. A. K. Miller and O. D. Sherby, *Acta Metall.*, 1978, vol. 26, pp. 298–304.
31. D. G. Morris and D. R. Harries, *Met. Sci.*, 1978, vol. 12, pp. 525–31.

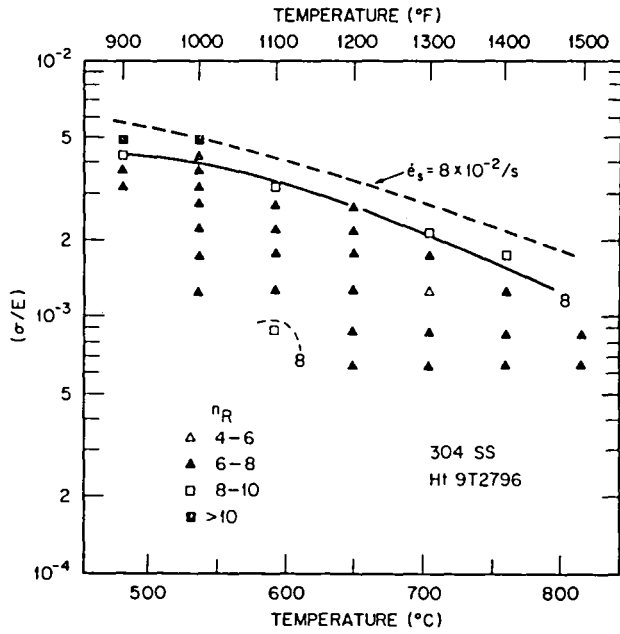


Fig. 1. Variation of the Stress Exponent for Rupture (n_R) with Modulus-Compensated Stress and Temperature.

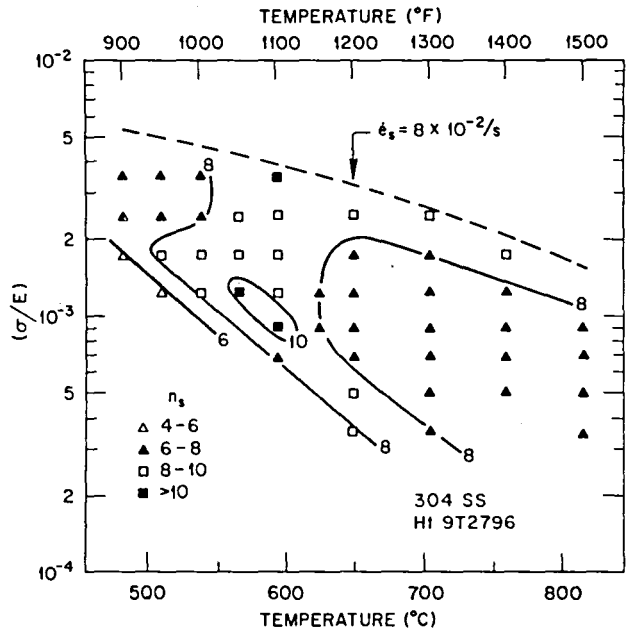


Fig. 2. Variation of the Stress Exponent for Secondary Creep Rate ($\dot{\epsilon}_s$) with Modulus-Compensated Stress and Temperature.

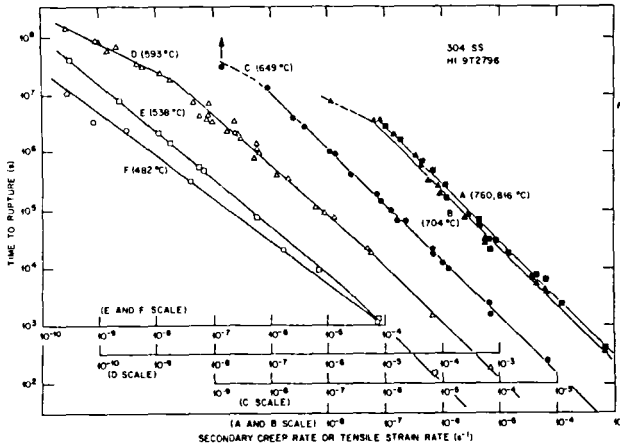


Fig. 3. Monkman-Grant Plots for Type 304 Stainless Steel at Temperatures from 482 to 816°C.

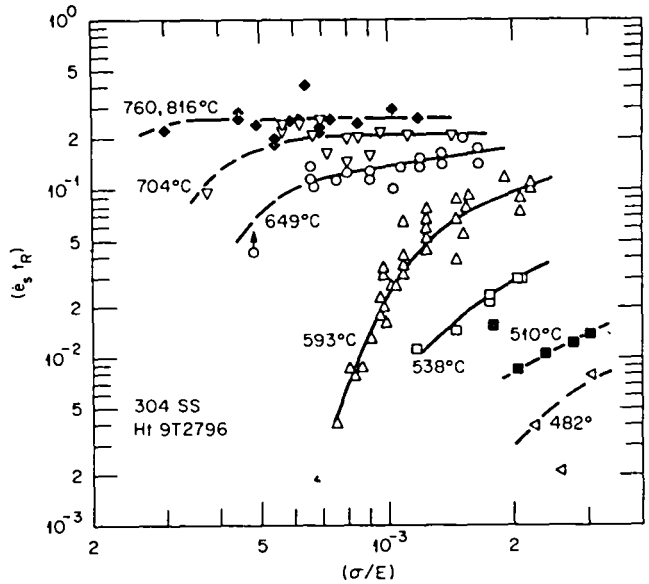


Fig. 4. Effects of Temperature on Linear Strain Parameter vs Modulus-Compensated Stress for Type 304 SS.

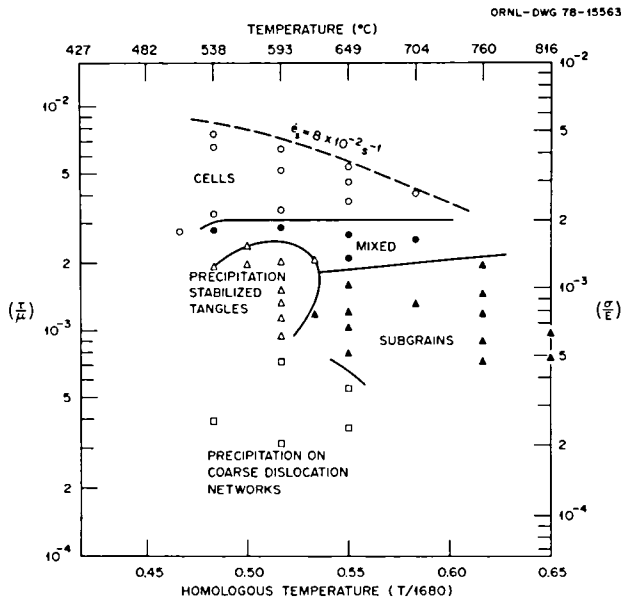


Fig. 5. Metallurgical Substructure Map for Type 304 Stainless Steel Heat 9T2796.

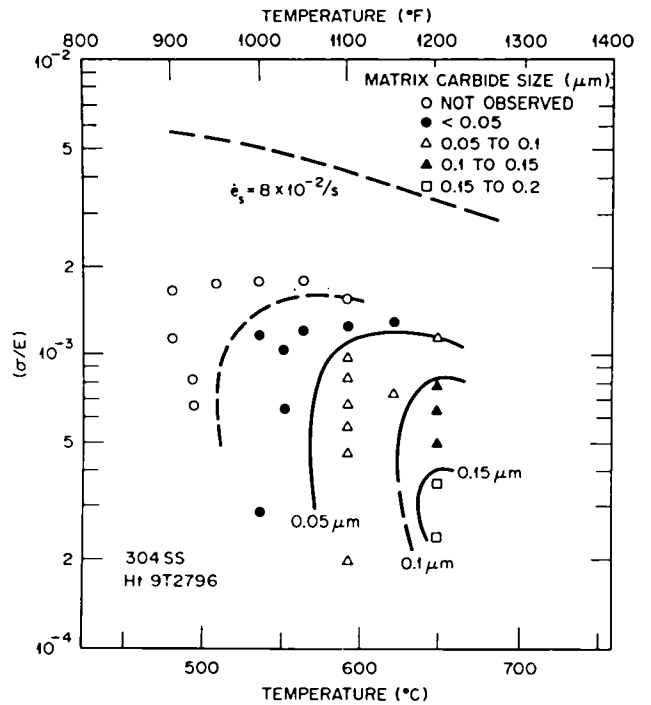


Fig. 6. Variation of Matrix Carbide Particle Size with Modulus-Compensated Stress and Temperature in Creep Tested Specimens

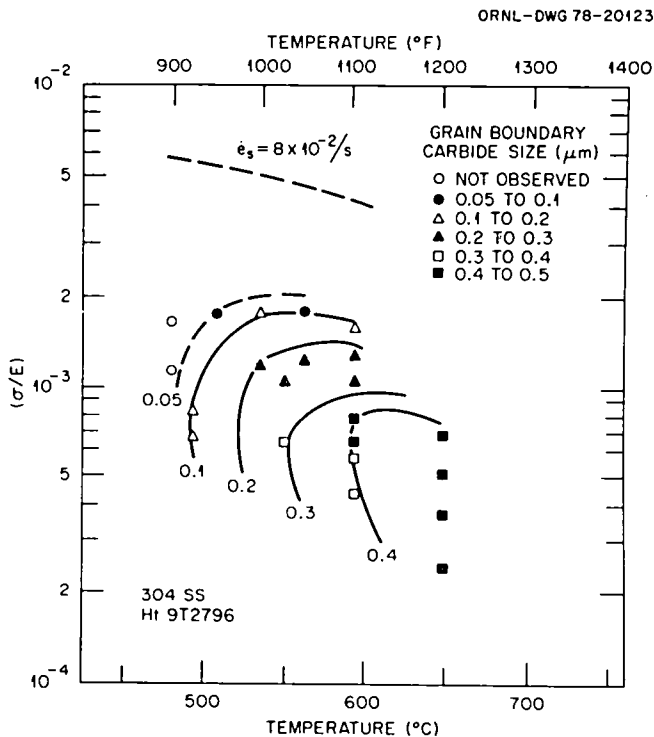


Fig. 7. Variation of Grain Boundary Carbide Particle Size with Modulus-Compensated Stress and Temperature in Creep Tested Specimens.

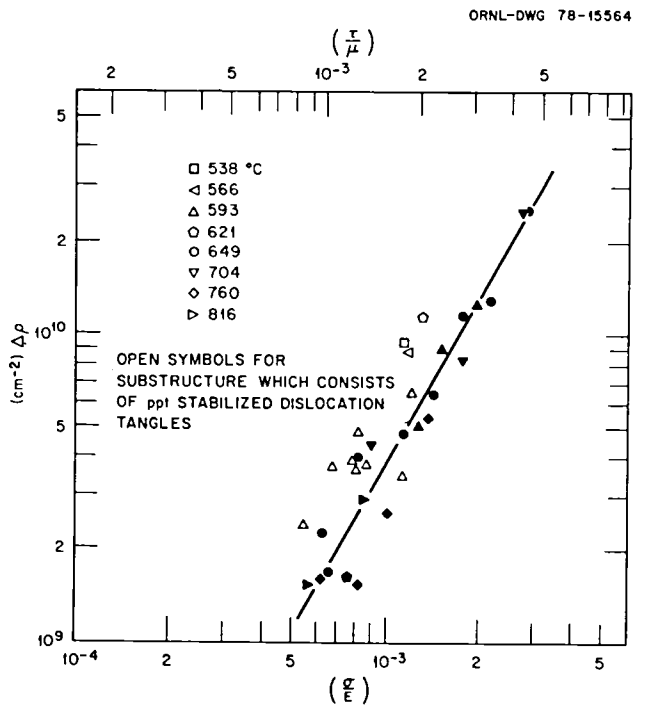


Fig. 8. Change in Dislocation Density vs Modulus-Compensated Stress for Creep and Tensile Specimens.